JCTC Journal of Chemical Theory and Computation

pubs.acs.org/JCTC Article

Surface Adsorption at the Thermodynamic Limit Using Periodic DLPNO-MP2 Theory: A Study of CO on MgO at Dilute and Dense Coverages

Andrew Zhu, Poramas Komonvasee, Arman Nejad, and David P. Tew*

Cite This: J. Chem. Theory Comput. 2026, 22, 3927−3936 Read Online

ABSTRACT: We apply periodic domain-based local pair natural orbital second-order Møller−Plesset perturbation theory (DLPNO-MP2) to probe the adsorption energy of CO on MgO(001), the consensus model system for surface adsorption. A number of robust correlated wavefunction methods now achieve excellent agreement with experiment for the adsorption of a single CO molecule onto the MgO surface. However, studies probing denser coverage ratios are scarce because of the increased computational expense and the larger configuration space needed for optimization. We leveraged the computational efficiency of periodic DLPNO-MP2 to perform simulations beyond a single unit cell. By using large supercells, we highlight the importance of accurately representing the thermodynamic limit of the surface and demonstrate in turn that different coverage ratios can be consistently probed. In the dilute regime, we show that the adsorption energies obtained from periodic DLPNO-MP2 agree with existing benchmarks. We then obtain adsorption energies at increasing densities, approaching full monolayer coverage. Our results show a reduction in binding strength at full coverage, agreeing with experimental observations, which is explained by the increasing lateral repulsions between the COs. This study demonstrates the efficacy of periodic DLPNO-MP2 for probing increasingly sophisticated adsorption systems at the thermodynamic limit.

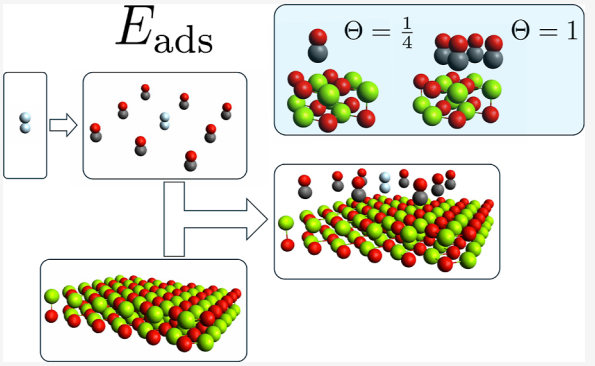

1. INTRODUCTION

The interaction of a molecule as it adsorbs onto a surface is a key chemical phenomenon, where accurate modeling provides benefits for a number of important applications. In particular, computational evaluation of the adsorption energy gives mechanistic insight into reactions for heterogeneous catalysis, gas storage, and surface lubrication, among others.[1−8] Electronic structure studies of adsorption systems have predominantly employed density functional theory (DFT), due to its computational efficiency. However, accurate modeling of the dispersion interactions involved is difficult unless semiempirical corrections are incorporated into the density functional treatment. This has prompted the development of a range of dispersion-corrected functionals,[9−15] incorporating varying degrees of many body dispersion (MBD), which have shown to be successful in describing adsorption interactions. In spite of this, to gain further insight into the uncertainties between different functionals, benchmarking against higher accuracy and systematically improvable correlated wavefunction methods, which inherently capture dispersive effects, is needed to provide reliable interaction energies. This in turn facilitates the development of improved future functionals.

The adsorption of a single carbon monoxide (CO) molecule onto a pristine magnesium oxide (MgO(001)) surface has become the consensus toy model system to probe surface adsorption interactions. Computational schemes can be roughly divided into finite-cluster methods or approaches employing periodic boundary conditions. Recently, a number of studies, employing high accuracy correlated wavefunction methods, including second-order Møller−Plesset perturbation theory (MP2) and coupled cluster theory with singles, doubles and perturbative triples excitations (CCSD(T)), have obtained excellent agreement for the adsorption energy of CO on MgO at the dilute coverage limit.[16−19] Alessio et al.[17] and Boese and Sauer[16] both employ hybrid MP2: DFT-D embedded cluster calculations, incorporating single point CCSD(T) calculations, to obtain the final adsorption energy estimate, with values of -21.2 ± 0.5 kJ mol^{-1} and -21.0 ± 1.0 kJ mol^{-1}, respectively. Alessio et al. also employ periodic local MP2 to demonstrate

Received: December 31, 2025
Revised: February 26, 2026
Accepted: April 1, 2026
Published: April 13, 2026

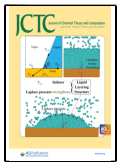

agreement with their embedded cluster MP2 estimates. Shi et al.[18] used CCSD(T) calculations within their embedded cluster SKZCAM approach, obtaining an adsorption energy of -19.2 ± 1.0 kJ mol^{-1}, which they show agreement with canonical periodic CCSD(T) and diffusion Monte Carlo. Finally, Ye and Berkelbach[19] calculate adsorption energies using periodic local natural orbital (LNO) schemes at MP2 and CCSD(T) levels, calculating a value of -20.0 ± 0.5 kJ mol^{-1}. Considering the touted standard of "chemical accuracy" is 4.2 kJ mol^{-1}, the overall consensus of these methods is remarkable, considering the differences in the approaches taken and the need to converge out errors in all the method-specific wavefunction and basis-related parameters, as well as finite-size effects. In contrast to these correlated wavefunction methods, Ye and Berkelbach[19] and Shi et al.[18] show that, for this prototypical system, lower-cost approaches such as DFT-D3, DFT-MBD, and random-phase approximation[20,21] fail to achieve results which agree within this threshold. This exemplifies the importance of employing high accuracy wavefunction schemes to form robust benchmark energies.

Experimental enthalpies for CO on MgO(001) adsorption have been determined using temperature-programmed desorption (TPD) techniques, of which we highlight the work from Dohnálek et al.[22] and Wichtendahl et al.[23] Both studies produce TPD spectra at varying CO coverage ratios (Θ), reporting desorption values at minimal densities of around $\frac{1}{4}$ monolayer coverage, which provide the closest estimate to the adsorption energy at the dilute limit. Using these experimental references, previous computational works have conducted analyses to compute comparable adsorption energy values, by accounting for thermal and zero-point energy contributions, the PV term, and the pre-exponential factor used in the Redhead equation.[24] Boese and Sauer obtained a TPD-derived energy of (-20.6 ± 2.4) kJ mol^{-1}, while Shi et al. obtained an experimental estimate of (-19.2 ± 1.0) kJ mol^{-1}. With both experiment-derived and theoretical studies from a number of different works agreeing well within chemical accuracy, the adsorption energy of CO on MgO at the dilute regime appears to have reached a robust consensus, providing a rigorous benchmark.

There are, however, still unanswered questions about simulating adsorption processes. In real chemical conditions, adsorption reactions rarely feature a single adsorbate molecule, and consideration for the optimal ratio of surface site availability is a key concern for heterogeneous catalysis. For example, experimental literature for CO adsorption onto an MgO surface reports varying reactivities associated with dilute to dense coverage regimes.[22,23,25−27] While an agreed benchmark for the adsorption energy of a single CO molecule on a pristine MgO surface has now been established, simulations incorporating multiple CO adsorption sites at denser monolayer coverages are still scarce. These systems are inherently more difficult to simulate, given the expanded configuration space to now optimize over and the need to incorporate lateral interactions between the adsorbate monomers. For these larger adsorption unit cells or fragments, simulating the in-principle infinite extent of the surface or the thermodynamic bulk limit becomes increasingly important in order to remove finite size errors or edge effects. Looking at other adsorption systems, we highlight the work from Usvyat,[28] who investigated dense Argon monolayers on MgO(100), as one of the few schemes using correlated wavefunction methods. All in all, the increased computational demand required to simulate larger surface systems poses a steep challenge for current correlated wavefunction methods.

Recently, we have outlined the theory and implementation of two complementary methods for periodic domain-based local pair natural orbital (DLPNO) second-order Møller−Plesset perturbation theory (MP2).[29,30] These implementations form the foundation in the development of higher accuracy correlated methods such as periodic DLPNO−CCSD(T). DLPNO schemes enable vast compression of the virtual space, enabling calculations of large supercells to accurately extrapolate to the thermodynamic limit. In this contribution, we use periodic DLPNO-MP2 to probe CO on MgO(001) adsorption with large supercells beyond a single unit cell. We focus upon ensuring our calculations are converged with respect to the complete PNO space (CPS) limit, the complete basis set (CBS) limit, and the thermodynamic limit of the surface. This study provides the first demonstration that linear-scaling DLPNO-MP2 can yield surface interaction energies that are converged with respect to all three limits. This capability enables us to robustly probe the adsorption energies at different CO coverage densities, including denser coverage regimes, where the lateral interactions in the presence of the thermodynamic bulk of the surface have never previously been explored.

First, we outline our computational methodology employing periodic DLPNO-MP2 to model surface adsorption systems. Then, in Section III, we verify the validity of DLPNO-MP2 for surface interactions by evaluating the adsorption energy toward the infinitely dilute regime, which can be benchmarked rigorously against the aforementioned schemes. Having established agreement, we then use periodic DLPNO-MP2 to probe CO coverage ratios approaching the fully filled monolayer ($\Theta = 1$) limit in Section IV. This is achieved through leveraging the computational efficiency of periodic DLPNO-MP2, enabling simulation of multiple adsorption sites within a supercell, while ensuring the thermodynamic limit of the surface is probed. In doing so, we have conducted some of the largest supercell calculations to probe surface adsorption using correlated wavefunction schemes.

2. METHODS

2.1. Periodic DLPNO-MP2

DLPNO theory[31,32] is an established method within molecular quantum chemistry to reduce the computational cost of correlated wavefunction schemes, achieving near-linear scaling of computational effort with system size with only modest loss in accuracy by replacing integrals and excitation amplitudes with low-rank approximations that exploit the inherent locality of electron correlation in insulators. Our two works, BvK-DLPNO-MP2 and Megacell-DLPNO-MP2, represent the first full adaptations of DLPNO theory to periodic systems.

Our "BvK" scheme employs Born−von Kármán (BvK) boundary conditions,[29] while the "Megacell" method retains rigorous translational symmetry but exchanges the lattice summation in the BvK integrals with explicit sums over direct−space interactions.[30] Both implementations converge to the same values at the thermodynamic limit and also show excellent agreement with canonical benchmarks. The degree of compression through the PNOs is controlled through a single variable, the occupation number threshold, $\mathcal{T}_{\mathrm{PNO}}$, where the error incurred due to discarding virtuals is proportional to $\sqrt{\mathcal{T}_{\mathrm{PNO}}}$. We demonstrate numerically that the pilot scheme of Megacell-DLPNO-MP2 is particularly computationally efficient with near-linear scaling with respect to supercell size. Our aim in this contribution is to use Megacell-DLPNO-MP2 to reveal further insight into interactions

https://doi.org/10.1021/acs.jctc.5c02179
J. Chem. Theory Comput. 2026, 22, 3927−3936

of the MgO + CO adsorption system. Previous computational studies of the surface adsorption energy of CO on MgO have incorporated higher accuracy correlated wavefunction methods, notably CCSD(T). While our study employs only MP2, we note that previous work demonstrates that MP2 is almost as accurate as CCSD(T) for these interactions,[14,19,33] suggesting significant value in a periodic MP2 method that can efficiently simulate the thermodynamic bulk of the surface layer in an adsorption reaction.

The efficacy of periodic DLPNO-MP2 enables multiple unit cells, each featuring a CO adsorption site, to be simulated. Figure 1 presents unit cells corresponding to coverage ratios of $\Theta = \frac{1}{4}$ and $\frac{1}{9}$, respectively, as well as 3 × 3 supercells of each system, where the CO molecule in the reference (central) unit cells is highlighted in white. By simulating more than a single unit cell (Gamma point), our calculations using Megacell-DLPNO-MP2 ensure that the adsorbed molecule in the reference cell has an interaction length scale with the surface that can extend beyond the boundaries of the unit cell. This ensures that the correct thermodynamic limit of the bulk surface is always being probed. In turn, the accurate evaluation of the different coverage ratios can then be controlled by the size of the surface slab and the number of adsorbates within the unit cell. In this contribution, we predominantly employ 3 × 3 supercells, using 5 × 5 supercells occasionally to verify the thermodynamic limit convergence of our calculations. We believe this work is the first instance where a periodic post-HF scheme simulates multiple adsorption sites in a periodic supercell calculation, in contrast to previous studies, which employ only single unit cells or Gamma point calculations.

2.2. Evaluation of Adsorption Energy

The adsorption energy is defined as the energy difference, per unit cell, between the adsorbed CO molecule on the MgO surface and the energies of the individual noninteracting components

$$E_{\text{ads}} = E^{\text{crys,eq}}_{[\text{MgOCO}]} - E^{\text{crys,eq}}_{[\text{MgO}]} - E^{\text{mol,eq}}_{[\text{CO}]} \tag{1}$$

where [MgO] is the pristine MgO surface and [CO] is the isolated gas-phase CO molecule, and each energy is evaluated at the fully relaxed equilibrium structure. In line with previous work,[17−19] we decompose E_{ads} into

$$E_{\text{ads}} = E_{\text{int}} + \Delta_{\text{geom}} \tag{2}$$

where E_{int} is the interaction energy of CO and MgO, computed using MgO and CO geometries frozen at those of the CO + MgO system, and Δ_{geom} is the energy change upon relaxing to the geometries of pristine MgO and gas-phase CO. E_{int} is computed with counterpoise correction to reduce basis set superposition error (BSSE)

$$E_{\text{int}} = E'_{\text{int}} + \Delta E^{\text{crys}}_{[\text{CO}]} \tag{3}$$

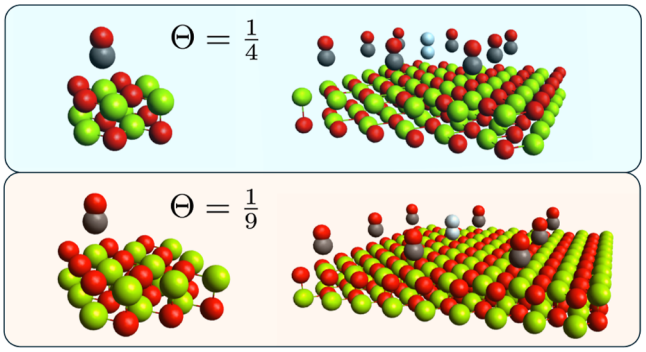

Figure 1. Unit cell structures for CO adsorption on an MgO surface corresponding to coverage ratios of $\Theta = \frac{1}{4}$ (top) and $\Theta = \frac{1}{9}$ (bottom). The unit cells are depicted on the left, the 3 × 3 supercells on the right where the central cell CO molecule is highlighted.

$$E'_{\text{int}} = E^{\text{crys}}_{[\text{MgOCO}]} - E^{\text{crys}}_{[\text{MgO},\overline{\text{CO}}]} - E^{\text{crys}}_{[\text{CO},\overline{\text{MgO}}]} \tag{4}$$

$$\Delta E^{\text{crys}}_{[\text{CO}]} = +E^{\text{crys}}_{[\text{CO}]} - E^{\text{mol}}_{[\text{CO},\overline{\text{CO}}]} \tag{5}$$

Here, a system $[X, \overline{Y}]$ denotes the X subsystem with ghost functions representing $\overline{Y}$. The second term $\Delta E^{\text{crys}}_{[\text{CO}]}$ accounts for the lateral interactions between CO molecules and is the difference between a periodic calculation of the CO lattice and a molecular calculation using ghost functions at the lattice sites. Many previous works approximate $E_{\text{int}} \approx E'_{\text{int}}$, neglecting the second term, which is indeed insignificant at dilute CO coverage. We are interested in examining the dense coverage regime where this term becomes significant. Figure 2 shows a schematic visualizing the contributions within E_{int}. The final adsorption energy in this paper is thus given by

$$E_{\text{ads}} = E'_{\text{int}} + \Delta E^{\text{crys}}_{[\text{CO}]} + \Delta_{\text{geom}} \tag{6}$$

Ye and Berkelbach[19] and Shi et al.[18] both compute Δ_{geom} using informed choices of DFT functionals, incorporating dispersion corrections, reaching a similar agreement of approximately 1.0 kJ mol^{-1} for dilute coverages.

2.3. Computational Details

Within our study, Megacell-DLPNO-MP2 is employed to evaluate all quantities contributing to E_{int}, apart from $E^{\text{mol}}_{[\text{CO},\overline{\text{CO}}]}$. This calculation is aperiodic, featuring only a single CO molecule surrounded by ghost functions, which we compute using the existing molecular DLPNO-MP2 implementations[34,35] in the pnoccsd module, within the TURBOMOLE program. The HF orbitals for this system are obtained from the ridft module.

Megacell-DLPNO-MP2[30] has been implemented in a developmental version of the TURBOMOLE[36] program, within the pnoccsd module.[34,35,37,38] Periodic LCAO-based HF calculations using k-point sampling have recently become available on developmental branches of TURBOMOLE, in the riper module,[39−44] the output of which provides the HF Bloch functions and band energies required for MP2. The RI-J approximation is employed, and we adopt the Monkhorst−Pack grid for our k-point grid.[45] We use our recently developed Wannier function (WF) localization procedure to prepare localized occupied orbitals.[46] As described in ref 30, Megacell-DLPNO-MP2 embeds a supercell correlation treatment within a larger megacell in order to ensure all correlated WFs are sufficiently decayed. Periodic HF calculations are performed on a k-grid spanning the size of the megacell, which is related to the supercell size by $k_{\text{mega}} = 2k_{\text{super}} - 1$ in each Cartesian dimension.

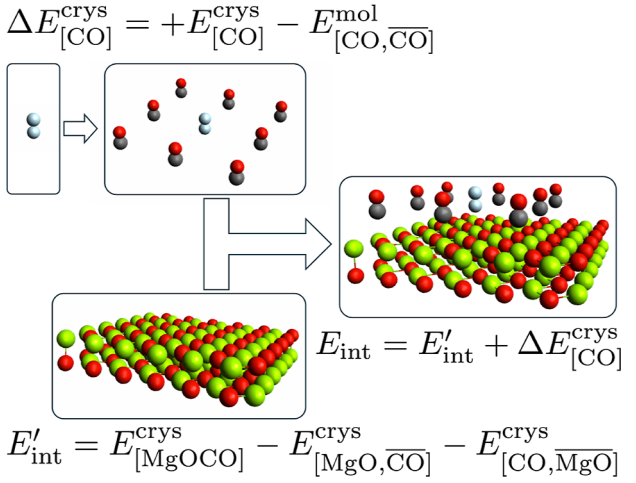

Figure 2. Contributions to the adsorption energy of CO on the MgO surface, for any given coverage ratio. The lateral interactions of the gas-phase CO molecules must be added to E_{int} to properly distinguish adsorption energies at different coverage ratios.

https://doi.org/10.1021/acs.jctc.5c02179
J. Chem. Theory Comput. 2026, 22, 3927−3936

Previous work from Shi et al.[18] highlights the underestimation of E_{int} if correlation from the 2s 2p orbitals on magnesium is neglected. We therefore only freeze the 1s core−shells for C, O, and Mg in our DLPNO-MP2 treatment. In our investigation for the dilute regime, we directly use the optimized unit cell geometries reported by Ye and Berkelbach,[19] which we describe in greater detail in Section III. A pristine surface of MgO is employed for the dense coverage calculations. All unit cell geometries are reported in the Supporting Information.

All calculations were run on a single node (Intel(R) Xeon(R) Gold 6248R CPU) with a maximum RAM limit of 386 GB and 1.8 TB disk, with an OMP parallelization of up to 48 threads. No single calculation in this contribution exceeded a wall time of 24 h, highlighting the efficiency of the Megacell-DLPNO-MP2 approach. Our largest calculations featured supercells containing just under 30,000 orbital basis functions, representing the largest calculations undertaken by Megacell-DLPNO-MP2 thus far.

2.4. Basis Set

The importance of using sufficiently expansive basis sets to capture adsorption interactions has been highlighted extensively in previous works. In the initial phase of testing, we encountered issues converging the periodic HF calculations using all-electron cc-pVTZ orbital basis sets,[47,48] which we attributed to linear dependency issues arising from the diffuse basis functions centered on Mg, leading to divergent exchange contributions. HF convergence using the all-electron pob-TZVP[49] and pob-TZVP-rev2[50,51] basis sets presented no issues. However, diffuse and additional polarization functions are vital for accurately capturing the dispersion interactions in adsorption systems but are absent from these reduced basis sets. Our solution was to employ the cc-pVXZ orbital basis sets for C and O and to use modified pob-XZVP-rev2 basis sets for Mg (X = D,T). These modified basis sets contained additional valence polarization and diffuse functions from the cc-pVXZ basis sets as well as core polarization functions from the cc-pwCVXZ basis sets. We thus performed two sets of adsorption calculations, using approximate "DZ" and "TZ" quality basis sets, enabling an estimate of the complete basis set limit values. The basis sets employed are listed in the Supporting Information.

For the RI-J approximation within the periodic HF calculations, the cc-pVTZ auxiliary basis sets[52] were employed for carbon and oxygen atoms, while the def2-TZVP auxiliary basis sets[52] were used for magnesium, for all calculations. The same auxiliary basis sets were also employed for the density-fitting treatment within the MP2 calculations, apart from those for the ghost atoms, which did not feature any auxiliary basis functions.

2.5. Canonical and Basis Set Extrapolations

In order to provide a meaningful comparison with other theoretical and experimental adsorption energies, our results are extrapolated to the respective canonical and basis set limits. For each individual quantity contributing to E_{int}, DLPNO-MP2 calculations are performed at two occupation number thresholds ($\mathcal{T}_{PNO} = 10^{-7}$, 10^{-8}), with both the "DZ" and "TZ" basis sets. For each basis set, a square root extrapolation to estimate the complete PNO space (CPS) limit[53,54] is first performed

$$E_{corr,CPS} = \frac{\mathcal{T}_2^{1/2}E(\mathcal{T}_1) - \mathcal{T}_1^{1/2}E(\mathcal{T}_2)}{\mathcal{T}_2^{1/2} - \mathcal{T}_1^{1/2}} \quad (7)$$

Here, $E(\mathcal{T}_1)$ and $E(\mathcal{T}_2)$ are DLPNO-MP2 correlation energies obtained at two occupation number thresholds, where $\mathcal{T}_1 > \mathcal{T}_2$. With these CPS estimates, the correlation energy estimate at the complete basis set (CBS) limit is then obtained through Helgaker's two-point extrapolation[55,56]

$$E_{corr,CBS} = \frac{X^3E(X) - Y^3E(Y)}{X^3 - Y^3} \quad (8)$$

where X and $Y = X - 1$ refer to the cardinality of the basis sets used. We then computed E_{int} from eq 3. The dominant source of uncertainty arises from the basis set extrapolation. We also compute a E_{int} value using the $E_{corr,TZ}$ correlation energies and define the uncertainty as half the difference between this value and the basis set extrapolated E_{int} energy. Finally, the total DLPNO-MP2 interaction energy is evaluated by summing the extrapolated correlation contribution to the HF energies, which are computed in the "TZ" basis.

3. TOWARD THE DILUTE COVERAGE LIMIT

In this section, we study the adsorption of a single CO molecule on the pristine MgO surface, modeling the surface at the thermodynamic limit and probing the adsorption energy toward the infinitely dilute limit. We follow similar protocols to Ye and Berkelbach[19] and Shi et al.,[18] who model the MgO(001) surface using a two-layer slab, which both studies conclude is sufficient to converge the adsorption energy with respect to the layer depth. The CO molecule is adsorbed in a perpendicular fashion to the surface, with the C end pointing toward the 5-fold coordinated Mg site, with a Mg−C interaction distance set to 2.460 Å, to enable direct comparison with the aforementioned two works.

We employ three types of unit cell to probe the dilute regime: a $2 \cdot 2$, $3 \cdot 3$, and $4 \cdot 4$ surface slab of 2-layer MgO, corresponding to surface coverages of $\Theta = \frac{1}{4}$, $\frac{1}{9}$, and $\frac{1}{16}$. $2 \cdot 2$ and $3 \cdot 3$ unit cells are presented in Figure 1. Our chosen geometries are taken directly from the optimized equilibrium structures reported by Ye and Berkelbach,[19] which they obtain through geometry optimization with the Perdew−Burke−Ernzerhof[57] (PBE) functional with D3 dispersion treatment,[10] fixing the bottom layer surface slab. They report a single geometry relaxation energy from all surface slab optimizations, Δ_{geom}, of 1.1 kJ mol^{-1}, and we thus adopt the same value. The crucial difference with our study is that our supercell periodic approach can independently examine different coverage ratios while also converging the thermodynamic limit of the surface through increasing the supercell size.

3.1. Dilute Regime Results

We first verified the thermodynamic limit convergence of the adsorption calculations. Table 1 presents the HF and correlation energy contributions to the interaction energy for the $2 \cdot 2$ surface slab unit cell at "TZ" quality, for supercell sizes of 3×3 and 5×5. The correlation energies are computed at two $\mathcal{T}_{PNO}$ thresholds, which are then used to estimate the CPS limit using a square root extrapolation.[53,54] MP2 energies, summing the HF and CPS values, are also given. The full

Table 1. Hartree−Fock and Correlation Energy Contributions to E'_{int} and E_{int}, Comparing Supercell Sizes of 3×3 and 5×5[a]

k_{super}	E'_{int}		E_{int}	
	3×3	5×5	3×3	5×5
HF	2.13	2.13	2.47	2.47
$E_{corr}(\mathcal{T}_{PNO} = 10^{-7})$	−17.71	−17.79	−18.42	−18.51
$E_{corr}(\mathcal{T}_{PNO} = 10^{-8})$	−18.26	−18.38	−18.97	−19.11
E_{corr} (CPS)	−18.52	−18.66	−19.23	−19.39
MP2 (CPS)	−16.38	−16.53	−16.76	−16.91

[a]Energies are given in kJ mol^{-1}. Calculations employed the 2×2 surface slab unit cell, using the modified "TZ" basis set. Total MP2 interaction energies are given, as the sum of the HF and CPS correlation energy components.

https://doi.org/10.1021/acs.jctc.5c02179
J. Chem. Theory Comput. 2026, 22, 3927−3936

interaction energies, E_{int}, and the contribution ignoring CO lateral interactions, E'_{int}, are both presented.

Examining the HF energies, we first note that the 3 × 3 and 5 × 5 supercells correspond to HF calculations spanning the megacell, which uses *k*-grids of sizes 5 × 5 and 9 × 9, respectively. Agreement, to a precision of 0.01 kJ mol^{-1}, is achieved, indicating thermodynamic limit convergence. For correlation energies, including the extrapolated CPS limits, we note small deviations between the two supercell sizes, of magnitudes around 0.1 kJ mol^{-1}. The close agreement of these energies, especially when compared to the magnitude of uncertainty when converging to the basis set limit, which we subsequently discuss, allows us to conclude that both the thermodynamic limit of the surface slab and the canonical limit have been sufficiently converged. Comparing E_{int} and E'_{int}, we see that lateral interactions between CO molecules have a very small contribution to the overall correlation energy in this dilute regime, of less than 1 kJ mol^{-1}. Computing energies for the 3 · 3 and 4 · 4 surface slab unit cells at 5 × 5 supercell sizes is currently difficult due to the severe memory demands of these very large supercells, but given that the 2 · 2 unit cell represents the densest coverage ratio, we expect 3 × 3 supercells to also be sufficient for representing the thermodynamic limit for these unit cells.

Figure 3 presents the E_{int} energies at increasing coverage ratios, obtained from the 4 · 4, 3 · 3, and 2 · 2 surface slab unit cells, respectively. The top panel presents the HF energies, while the bottom plots the MP2 correlation energy contributions. For both cases, the cohesive energies for different coverage ratios are evaluated using the "DZ" and "TZ" basis sets. A 3 × 3 supercell was employed in all cases. For the MP2 correlation energies, an inverse cube extrapolation is performed to estimate the basis set limit value, using eq 8.

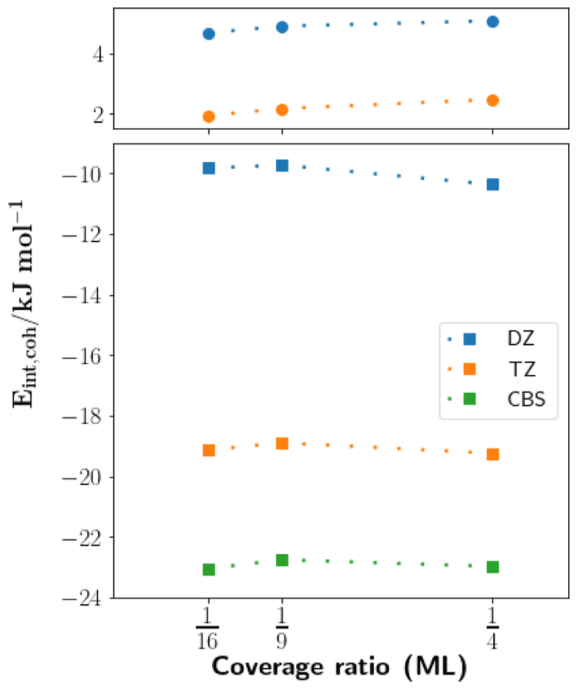

Figure 3. Hartree−Fock (top) and MP2 correlation energies (bottom) for $E_{int,coh}$, at three dilute coverage ratios. Results using the modified "DZ" and "TZ" basis sets are shown, and complete basis set estimate is provided for the MP2 correlation energies.

We first highlight that the cohesive energies are largely similar in magnitude across the different coverage ratios, indicating that all three coverage ratios capture the dilute coverage regime. While a slight increase in MP2 correlation energy is observed from $\frac{1}{4}$ to $\frac{1}{9}$ coverage ratios, this deviation is on a similar order of magnitude to the uncertainties incurred from the CPS and thermodynamic limit extrapolations and thus not significant. The HF cohesive energies show a very slight decrease toward further dilute coverages. The observation that all three ratios are within the same dilute regime agrees with the experimentally derived adsorption energies reported by Dohnálek et al.[22] They report, in Figure 4 of ref 22, an adsorption energy at $\frac{1}{4}$ coverage that is within 1 kJ mol^{-1} of their extrapolated adsorption energy at zero coverage.

For our method, we stress that the use of the 3 × 3 supercell size is crucial in obtaining the correct dependence with coverage ratio. This is because surface−adsorbate interactions extending beyond the length scale of the unit cell are explicitly considered in the supercell calculation, meaning that the thermodynamic limit of the surface is more accurately represented. In contrast, Ye and Berkelbach[19] perform single point (unit cell) calculations and report a significant decrease in correlation energy from the 2 · 2 to 4 · 4 unit cells with periodic MP2. We attribute this behavior to the growing surface slab size, which substantially increases the magnitude of the surface interaction if only one unit cell is considered. In the case of ref 19, where the motivation is to extrapolate to the infinitely dilute regime, this approach is completely valid. However, since we intend to discern differences between coverage ratios with Megacell-DLPNO-MP2, any interaction energy dependence on the surface slab size of the unit cell must be factored out. Calculations beyond a single unit cell are thus necessary in order to remove the finite size error associated with the surface.

Figure 3 shows that extrapolation of the "DZ" and "TZ" quality basis sets to a basis set limit estimate gives a significant decrease in MP2 correlation cohesive energies compared to the "TZ" values, on the order of 4 kJ mol^{-1}, across all coverage ratios. This source of error is the largest component of uncertainty within our scheme and is admittedly significantly larger than previous computational schemes, which we record in Table 2. As mentioned, we are currently prevented from

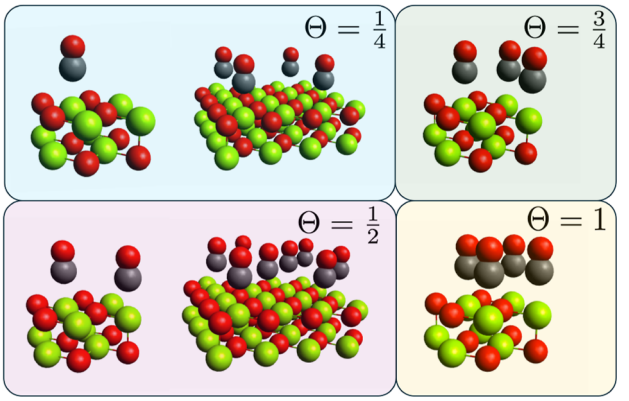

Figure 4. 2 × 2 and 4 × 4 surface slab unit cells used to probe adsorption coverage ratios toward the dense regime.

https://doi.org/10.1021/acs.jctc.5c02179
J. Chem. Theory Comput. 2026, 22, 3927−3936

Table 2. Comparison of Adsorption Energies of CO on the MgO(001) Surface Using Megacell-DLPNO-MP2 and Recent Results from the Literature at Various Surface Coverage Ratios (Θ)[a]

Θ	E_{ads} (kJ mol^{-1})	methodology
1/4	−19.4 ± 1.9	megacell-DLPNO-MP2
1/9	−19.5 ± 1.9	megacell-DLPNO-MP2
1/16	−20.0 ± 2.0	megacell-DLPNO-MP2
dilute limit	−21.2 ± 0.5	cl MP2/DFT-D+ΔCC[17]
dilute limit	−21.6 ± 0.3	pbc MP2[17]
1/8	−21.0 ± 1.0	cl MP2/DFT-D+ΔCC[16]
dilute limit	−18.8 ± 0.3	pbc MP2[19]
dilute limit	−20.0 ± 0.5	pbc CCSD(T)[19]
dilute limit	−18.5 ± 0.5	cl MP2[18]
dilute limit	−19.2 ± 0.6	cl CCSD(T)[18]
dilute limit	−20.6 ± 2.4	TPD[16]
dilute limit	−19.2 ± 1.0	TPD[18]

[a]"cl" and "pbc" refer to cluster and periodic wavefunction schemes, respectively. Experimental data from TPD spectroscopy[22,23] have been converted to adsorption energies in two different analyses.[16,18]

performing calculations using cc-pVTZ or higher quality basis sets due to our periodic HF. Work is currently underway to address these issues, which will enable calculations with QZ quality basis sets, to obtain narrower error bars, as demonstrated by Ye and Berkelbach.[19]

The final adsorption energies obtained via Megacell-DLPNO-MP2 are presented in Table 2, compared to previous periodic or cluster-based schemes as well as experimental TPD results. Our values are obtained by summing the HF energy for the "TZ" basis with the CBS extrapolated correlation energy. The three coverage ratios probed all fall within the dilute coverage regime, and we note the general excellent agreement of our values, within 2 kJ mol^{-1} of all other values presented in the Table. This is not surprising, given previous evidence of the good agreement of periodic and cluster MP2 calculations with higher-level coupled cluster results. Clearly, our larger error bars, obtained from halving the difference between the "TZ" and CBS extrapolated correlation energies, are a point of concern, stemming from our limitations in basis set. Despite this, the overall agreement of the scheme gives promise for Megacell-DLPNO-MP2 as a robust scheme to probe different adsorption coverages.

4. PROBING DENSE COVERAGES

While numerous wavefunction studies probing the adsorption energy of CO on MgO at the dilute coverage limit achieve excellent agreement with experimental values, considerably less work has been done to simulate the adsorption energy dependence at higher coverage ratios. From the perspective of simulations, the difficulty is now the vastly increased degrees of freedom that now need to be analyzed. Due to the lateral interactions between CO molecules, which are significant at higher coverage densities, differing (i.e., nonperpendicular) CO orientations and configurations need to be considered, in order to obtain the lowest energy state for a given coverage ratio. While some experiments give details of highly ordered c(4 × 2) phases[58,59] at ratios close to full monolayer coverage, relatively little consensus has been established for favored phases between $\frac{1}{4}$ and $\frac{3}{4}$ coverages, providing no benchmark systems for computational approaches. Dohnálek et al.[22] provide an experimentally derived adsorption energy plot as a function of CO coverage, which confirms a decrease in the magnitude of the adsorption energy toward full monolayer coverage, due to increasing CO lateral repulsions.

Cluster calculations are inherently disadvantaged, since modeling multiple CO adsorption sites to capture the CO lateral interactions involves building a much larger fragment. Recent work by Shi et al.[60] provides a solution by evaluating the cohesive energy of the lattice of COs in the absence of the surface at CCSD(T) accuracy and incorporating a correction for the effect of the MgO surface using DFT. However, lateral interactions under the effect of the surface are never directly explored to correlated wavefunction accuracy. Periodic approaches are more naturally suited to modeling denser coverage ratios, since the adsorbed layer increasingly resembles periodic models. However, large supercells beyond single unit cell calculations are required to correctly capture the full extent of the periodic lateral interactions. Furthermore, larger unit cells are needed if differing CO orientations or configurations are to be probed. Computational studies are scarce, but we highlight the work by Minot et al.,[61] using periodic Hartree−Fock, which report a combination of perpendicular and bent CO geometries at $\Theta = \frac{3}{4}$, presenting two different arrangements which are energetically comparable. To our knowledge, no correlated wavefunction studies, targeting denser coverage ratios, exist, and even studies with DFT are scarce.

In this section, we exploit the efficiency of Megacell-DLPNO-MP2 to simulate supercells with dense CO coverage. We choose not to explore the full parameter space involving nonperpendicular CO geometries or differing configurations, which would require a substantially more involved systematic study. Instead, we use Megacell-DLPNO-MP2 to simulate unit cells featuring perpendicular COs at increasingly dense coverage ratios approaching Θ = 1. Although not directly comparable to experimental TPD studies, we still expect to capture the effect of the lateral repulsions between COs with our simplified scheme and observe the decreasing magnitude of E_{ads}, toward Θ = 1.

We use a pristine version of the earlier 2 · 2 surface slab unit cell, employing the same Mg−C interaction distance as before. Since no geometry optimization has been performed, Δ_{geom} is zero. We populate the unit cells with one, two (separated diagonally), three, and four CO adsorption sites, in order to capture coverage ratios of $\frac{1}{4}$, $\frac{1}{2}$, $\frac{3}{4}$, and 1, respectively. We also utilize a pristine 4 · 4 surface slab unit cell, with 4 and 8 COs adsorption sites, to again probe $\frac{1}{4}$ and $\frac{1}{2}$ surface coverages, to verify the consistency of the E_{ads} calculations using Megacell-DLPNO-MP2. All unit cells employed are listed in Figure 4. A supercell size of 3 × 3 is used throughout, having confirmed the thermodynamic limit is correctly probed from Section III A. We use the same modified "DZ" and "TZ" basis sets as before. The calculations featuring 8 COs on a 4 · 4 surface represent the costliest calculations in this contribution, featuring just shy of 30,000 basis functions in the 3 × 3 supercell, with calculation wall times of 24 h.

With multiple CO adsorbates now in a given unit cell, the expression to evaluate the adsorption energy now needs to be modified

https://doi.org/10.1021/acs.jctc.5c02179
J. Chem. Theory Comput. 2026, 22, 3927−3936

$$E_{ads} = E_{int} = -E^{mol}_{[CO,\overline{CO}]} + \frac{E^{crys}_{[MgOCO]} - E^{crys}_{[MgO,\overline{CO}]} - E^{crys}_{[CO,\overline{MgO}]} + E^{crys}_{[CO]}}{n_{CO}} \quad (9)$$

where the first equality is due to the lack of geometry relaxation energy in this specific scheme. n_{CO} is the number of COs per unit cell, and $E^{mol}_{[CO,\overline{CO}]}$ is the energy of a single CO molecule, with ghost functions representing all remaining COs spanning the reference unit cell and the neighboring cells.

4.1. Dense Coverage Results

First, to confirm the validity of Megacell-DLPNO-MP2, we verify whether different unit cell choices, at a given coverage ratio, reproduce the same adsorption energy value. Again, we emphasize that the 3 × 3 supercell sizes used are crucial in accurately representing the thermodynamic bulk of the surface. This ensures that different unit cell surface slabs can give the same interaction energy. In Table 3, MP2 correlation energy values for E_{ads} at the same coverage ratios are given, for the 2 · 2 and 4 · 4 surface unit cells. Significant deviations, on the order of 2 kJ mol^{-1}, exist for PNO truncation thresholds of 10^{-6}, but they rapidly reduce to within 0.1 kJ mol^{-1} for 10^{-8}. From this, we can conclude that employing PNO truncation thresholds of up to 10^{-8} is necessary to obtain robust agreement with larger unit cells. HF energies are also presented, with no significant differences in energies between unit cells.

Figure 5 presents the adsorption energies of CO on the MgO surface, as a function of coverage ratio, up to the full monolayer ($\Theta = 1$), as blue squares. The contributions from HF, using the "TZ" basis, and MP2 correlation, at the CPS and basis set limit, are plotted as blue diamonds and circles, respectively. Pleasingly, the simulated adsorption energy values show an overall decrease in magnitude from $\Theta = \frac{1}{4}$ to $\Theta = 1$, with the least exothermic value of −10.3 kJ mol^{-1} at full monolayer coverage. This reflects the increased lateral repulsion between the CO molecules at higher ratios. One notes the larger increase in the HF repulsion, compared to the attractive dispersive correlation contribution, as the source of this overall behavior. In particular, we can attribute the marked increase in adsorption energy from $\Theta = \frac{1}{2}$ to $\Theta = \frac{3}{4}$ directly to the inclusion of nearest neighbor CO repulsions, which are present in the $\Theta = \frac{3}{4}$, 1 unit cells (see Figure 4). In comparison, we can reason that the diagonal neighbor CO lateral repulsions are much less significant, given the similar adsorption energies between $\Theta = \frac{1}{4}$ and $\Theta = \frac{1}{2}$. Unfortunately, the significant error bars, on the magnitude of around 2 kJ mol^{-1}, reiterate our current basis set limitations and highlight that further work is needed for all-electron basis sets for periodic systems.

Again, we reiterate caution in directly comparing to the TPD-derived adsorption energy curves presented by Dohnálek et al.[22] As mentioned before, our calculations do not consider nonperpendicular orientations or clusters of adsorbate molecules. Despite this, we do report a similar adsorption energy at full monolayer coverage, of around −10 kJ mol^{-1}, compared to Figure 4 in ref 22, although admittedly we have not simulated the c (4 × 2) phase that the authors report to be present. Further to this, the DLPNO-MP2 energy at $\Theta = \frac{3}{4}$ is notably smaller in magnitude than the experimental plot. We can posit that no nearest neighbor adsorption configurations can be responsible for the experimentally derived adsorption energies between $\Theta = \frac{1}{2}$ and $\frac{3}{4}$, since our calculations report significantly smaller magnitude adsorption energies. Overall, the qualitative behavior of the lateral repulsions, captured entirely within a consistent level of correlated wavefunction theory, indicates promise in simulating unit cells featuring multiple adsorption sites. With further improvements to Megacell-DLPNO-MP2, realistic simulation of even more sophisticated geometries appears feasible.

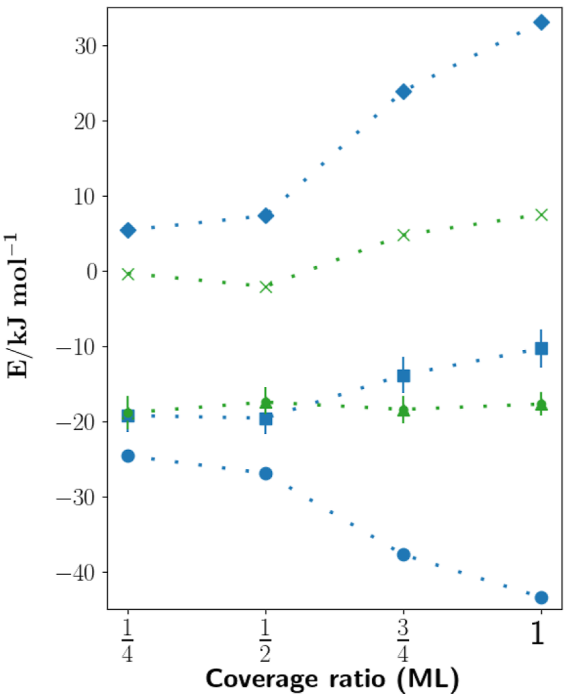

Figure 5. Total CO adsorption energies on the MgO surface at varying coverage ratios up to full monolayer coverage, plotted as blue squares, including error bars. The 2 · 2 surface slab unit cell is employed throughout. Hartree−Fock contributions, in the "TZ" basis, are plotted as blue diamonds. MP2 correlation energies contributions, extrapolated to the complete PNO space and basis set limits, are plotted as blue circles. The interaction energies without lateral contributions, E'_{int}, are plotted as green triangles. The gas-phase CO lateral interactions, ΔE_{CO}, are plotted as green crosses.

Table 3. Hartree−Fock and MP2 Correlation Energies for the Adsorption Energy (E_{ads}, in kJ mol^{-1}), Comparing the 2 · 2 and 4 · 4 Surface Slab Unit Cells, at $\frac{1}{4}$ and $\frac{1}{2}$ Coverage Ratios[a]

			DLPNO-MP2			
Θ	unit cell	HF	6	7	8	CPS
1/4	2 · 2	5.4	−20.0	−19.1	−19.9	−20.3
	4 · 4	5.4	−22.0	−19.5	−19.9	−20.1
1/2	2 · 2	7.3	−22.4	−21.9	−22.5	−22.7
	4 · 4	7.3	−23.3	−22.0	−22.4	−22.6

[a]All calculations used the "TZ" basis set. Different PNO truncation thresholds ($\mathcal{T}_{PNO} = 10^{-X}$, X = 6, 7, 8), including the complete PNO space extrapolation, are given.

https://doi.org/10.1021/acs.jctc.5c02179
J. Chem. Theory Comput. 2026, 22, 3927−3936

To quantify the impact of CO−CO interactions, we also compute the interaction energy without lateral contributions, E'_{int}. These values, also extrapolated to the complete PNO space and basis set limits, are plotted as green triangles in Figure 5. We see that the E'_{int} values are shown to be insensitive across coverage ratios. This demonstrates that inclusion of lateral interactions is crucial in order to correctly describe adsorption at denser regimes, and in Figure 5, these gas-phase lateral contributions are shown as green crosses. From the insensitivity of E'_{int}, we can also infer that the difference in lateral repulsion between the CO monomers in the gas phase, compared to that under the influence of the MgO surface, is negligible. This supports the consensus description of CO in MgO adsorption as a form of physisorption. In turn, it also validates the approach taken in ref 60, where the gas-phase CO interactions are used to approximate the cohesive contribution to the adsorption energy. However, for stronger adsorption interactions described by chemisorption,[62,63] we would expect a significant difference in lateral repulsions from the influence of the surface, and in those cases, our evaluation of E'_{int} would reveal insight into such character.

5. CONCLUSIONS

Correlated wavefunction approaches have been increasingly applied to study adsorption problems, of which CO adsorption on the MgO(001) surface is one of the most fundamental and commonly used case studies. Prior to this work, cluster and periodic wavefunction methods employing MP2 and coupled cluster theory have established excellent agreement with experimentally derived values for the adsorption energy of a single CO molecule onto a pristine MgO surface. In this work, we leverage the computational efficiency of periodic DLPNO-MP2 to push the scale of correlated wavefunction simulations on adsorption systems, modeling multiple unit cells featuring CO adsorption on MgO. In doing so, we demonstrate the surface slabs in our supercells are converged toward the thermodynamic limit, removing finite-size effects that enable accurate evaluation of adsorption energies across different coverage ratios.

We successfully demonstrate similar estimates of the dilute regime adsorption energy (∼− 20 kJ mol^{-1}), at three different coverage ratios, compared to previous computational and experimental approaches, validating the accuracy of Megacell-DLPNO-MP2. Tackling the adsorption energy of denser coverages is an inherently trickier problem due to the vastly larger configuration space that needs to be considered. Here, we employ a simple model consisting of perpendicularly adsorbed CO molecules, evaluating adsorption energies as a function of monolayer coverage ratio and considering the effect of the lateral repulsion between COs. We achieve agreement with the experiment of decreased exothermic behavior at higher coverage densities, approaching full monolayer coverage. Our current limitations in basis sets contributes the major source of error and highlights the continued need for improved Gaussian basis sets for periodic systems.[49,50,64,65] Overall, however, we show that periodic DLPNO-MP2 is a scalable and efficient approach to model a range of adsorption coverages at the thermodynamic limit, within an entirely consistent level of correlated wavefunction theory.

While the agreement between quantum chemistry and experimental methods for CO on MgO adsorption is impressive, further work is required to model realistic surface systems pertinent to heterogeneous catalysis. Surfaces are not completely pristine in true chemical conditions, and the presence of terraces, defects, and kinks on the surface are now understood to have significant influences on the binding with adsorbates.[66−73] Dohnálek et al.,[22] for example, report significantly more exothermic adsorption energies associated with defect-related sites, which become the dominant mechanism at extremely low coverages. Correlated wavefunction methods need to continue to improve to model increasingly large unit cells if these effects are to be captured. While approaches using DFT are common,[74−81] to our knowledge, there are significantly fewer studies employing correlated wavefunction methods. In this regard, we believe future versions of periodic DLPNO-MP2 will be a viable solution to explore sophisticated adsorption systems, treating periodic monolayer, defect, kink, or terraced surfaces all on equal footing, thanks to its computational efficiency. Work is currently ongoing to model different surface adsorbate systems, moving beyond the weakly physisorbed interactions dominant in CO on MgO, and ongoing method development toward a periodic PNO−CCSD(T) implementation will provide even greater accuracies for simulating systems of relevance to heterogeneous catalysis. Finally, periodic DLPNO schemes have the capability of providing higher accuracy training data for machine learning interatomic potentials,[82,83] which have been predominantly trained thus far on DFT.

■ ASSOCIATED CONTENT

Supporting Information

The Supporting Information is available free of charge at https://pubs.acs.org/doi/10.1021/acs.jctc.5c02179.

Unit cell geometries; basis sets; further results (PDF)

■ AUTHOR INFORMATION

Corresponding Author

David P. Tew − *University of Oxford, Oxford OX1 3QZ, U.K.*; orcid.org/0000-0002-3220-4177; Email: david.tew@chem.ox.ac.uk

Authors

Andrew Zhu − *University of Oxford, Oxford OX1 3QZ, U.K.*; orcid.org/0000-0001-7495-1528

Poramas Komonvasee − *University of Oxford, Oxford OX1 3QZ, U.K.*

Arman Nejad − *University of Oxford, Oxford OX1 3QZ, U.K.*; orcid.org/0000-0001-7241-186X

Complete contact information is available at: https://pubs.acs.org/10.1021/acs.jctc.5c02179

Notes

The authors declare no competing financial interest.

■ ACKNOWLEDGMENTS

Financial support for A.Z. from the University of Oxford and Turbomole GmbH is gratefully acknowledged. P.K. gratefully acknowledges funding through the Institute for the Promotion of Teaching Science and Technology. A.N. gratefully acknowledges funding through a Walter Benjamin Fellowship by the Deutsche Forschungsgemeinschaft (DFG, German Research Foundation) − 517466522.

REFERENCES

(1) Christensen, C. H.; Nørskov, J. K. A molecular view of heterogeneous catalysis. *J. Chem. Phys.* **2008**, *128*, 182503.
(2) Somorjai, G. A., "Active Sites in Heterogeneous Catalysis" in *Adv. Catal.*, Vol. *26* (Elsevier, 1977) pp 1−68.
(3) Chen, B. W. J.; Xu, L.; Mavrikakis, M. Computational Methods in Heterogeneous Catalysis. *Chem. Rev.* **2021**, *121*, 1007−1048.
(4) Ertl, G. Elementary Steps in Heterogeneous Catalysis. *Angew. Chem., Int. Ed. Engl.* **1990**, *29*, 1219−1227.
(5) Schauermann, S.; Nilius, N.; Shaikhutdinov, S.; Freund, H.-J. Nanoparticles for Heterogeneous Catalysis: New Mechanistic Insights. *Acc. Chem. Res.* **2013**, *46*, 1673−1681.
(6) Vogt, C.; Weckhuysen, B. M. The concept of active site in heterogeneous catalysis. *Nat. Rev. Chem.* **2022**, *6*, 89−111.
(7) Morris, R.; Wheatley, P. Gas Storage in Nanoporous Materials. *Angew. Chem. Int. Ed* **2008**, *47*, 4966−4981.
(8) Jahanmir, S.; Beltzer, M. An Adsorption Model for Friction in Boundary Lubrication. *A S L E Transactions* **1986**, *29*, 423−430.
(9) Grimme, S. Semiempirical GGA-type density functional constructed with a long-range dispersion correction. *J. Comput. Chem.* **2006**, *27*, 1787−1799.
(10) Grimme, S.; Antony, J.; Ehrlich, S.; Krieg, H. A consistent and accurate *ab initio* parametrization of density functional dispersion correction (DFT-D) for the 94 elements H-Pu. *J. Chem. Phys.* **2010**, *132*, 154104.
(11) Grimme, S. Density functional theory with London dispersion corrections. *WIREs Comput. Mol. Sci.* **2011**, *1*, 211−228.
(12) Tkatchenko, A.; Scheffler, M. Accurate Molecular Van Der Waals Interactions from Ground-State Electron Density and Free-Atom Reference Data. *Phys. Rev. Lett.* **2009**, *102*, 073005.
(13) Dion, M.; Rydberg, H.; Schröder, E.; Langreth, D. C.; Lundqvist, B. I. Van der Waals Density Functional for General Geometries. *Phys. Rev. Lett.* **2004**, *92*, 246401.
(14) Ugliengo, P.; Damin, A. Are dispersive forces relevant for CO adsorption on the MgO(001) surface? *Chem. Phys. Lett.* **2002**, *366*, 683−690.
(15) Maurer, R. J.; Ruiz, V. G.; Tkatchenko, A. Many-body dispersion effects in the binding of adsorbates on metal surfaces. *J. Chem. Phys.* **2015**, *143*, 102808.
(16) Boese, A. D.; Sauer, J. Accurate adsorption energies of small molecules on oxide surfaces: CO−MgO(001). *Phys. Chem. Chem. Phys.* **2013**, *15*, 16481−16493.
(17) Alessio, M.; Usvyat, D.; Sauer, J. Chemically Accurate Adsorption Energies: CO and H2O on the MgO(001) Surface. *J. Chem. Theory Comput.* **2019**, *15*, 1329−1344.
(18) Shi, B. X.; Zen, A.; Kapil, V.; Nagy, Péter R.; Grüneis, A.; Michaelides, A. Many-Body Methods for Surface Chemistry Come of Age: Achieving Consensus with Experiments. *J. Am. Chem. Soc.* **2023**, *145*, 25372−25381.
(19) Ye, H.-Z.; Berkelbach, T. C. Adsorption and vibrational spectroscopy of CO on the surface of MgO from periodic local coupled-cluster theory. *Faraday Discuss.* **2024**, *254*, 628−640.
(20) Bajdich, M.; Nørskov, J. K.; Vojvodic, A. Surface energetics of alkaline-earth metal oxides: Trends in stability and adsorption of small molecules. *Phys. Rev. B* **2015**, *91*, 155401.
(21) Mazheika, A.; Levchenko, S. V. Ni substitutional defects in bulk and at the (001) surface of mgo from first-principles calculations. *J. Phys. Chem. C* **2016**, *120*, 26934−26944.
(22) Dohnálek, Z.; Kimmel, G. A.; Joyce, S. A.; Ayotte, P.; Smith, R. S.; Kay, B. D. Physisorption of CO on the MgO(100) Surface. *J. Phys. Chem. B* **2001**, *105*, 3747−3751.
(23) Wichtendahl, R.; Rodriguez-Rodrigo, M.; Härtel, U.; Kuhlenbeck, H.; Freund, H.-J. Thermodesorption of CO and NO from Vacuum-Cleaved NiO(100) and MgO(100). *physica status solidi (a)* **1999**, *173*, 93−100.
(24) Redhead, P. A. Thermal desorption of gases. *Vacuum* **1962**, *12*, 203−211.
(25) Shigeishi, R. A.; King, D. A. Chemisorption of carbon monoxide on platinum {111}: Reflection-absorption infrared spectroscopy. *Surf. Sci.* **1976**, *58*, 379−396.
(26) Tait, S. L.; Dohnálek, Z.; Campbell, C. T.; Kay, B. D. n -alkanes on Pt(111) and on C(0001)Pt(111): Chain length dependence of kinetic desorption parameters. *J. Chem. Phys.* **2006**, *125*, 234308.
(27) Schmid, M.; Parkinson, G. S.; Diebold, U. Analysis of Temperature-Programmed Desorption via Equilibrium Thermodynamics. *ACS Phys. Chem. Au* **2023**, *3*, 44−62.
(28) Usvyat, D.; Sadeghian, K.; Maschio, L.; Schütz, M. Geometrical frustration of an argon monolayer adsorbed on the mgo (100) surface: An accurate periodic ab initio study. *Phys. Rev. B* **2012**, *86*, 045412.
(29) Nejad, A.; Zhu, A.; Sorathia, K.; Tew, D. P. DLPNO-MP2 for periodic systems. I. Periodic boundary conditions. *J. Chem. Phys.* **2025**, *163*, 214107.
(30) Zhu, A.; Nejad, A.; Komonvasee, P.; Sorathia, K.; Tew, D. P. DLPNO-MP2 for periodic systems. II. Megacell embedding. *J. Chem. Phys.* **2025**, *163*, 214108.
(31) Neese, F.; Hansen, A.; Liakos, D. G. Efficient and accurate approximations to the local coupled cluster singles doubles method using a truncated pair natural orbital basis. *J. Chem. Phys.* **2009**, *131*, 064103.
(32) Riplinger, C.; Neese, F. An efficient and near linear scaling pair natural orbital based local coupled cluster method. *J. Chem. Phys.* **2013**, *138*, 034106.
(33) Herschend, B.; Baudin, M.; Hermansson, K. Influence of Substrate Dynamics on COMgO(001) BondingUsing Molecular Dynamics Snapshots in Quantum-Chemical Calculations. *J. Phys. Chem. B* **2006**, *110*, 5473−5479.
(34) Schmitz, G.; Helmich, B.; Hättig, C. A scaling PNO−MP2 method using a hybrid OSV−PNO approach with an iterative direct generation of OSVs. *Mol. Phys.* **2013**, *111*, 2463−2476.
(35) Tew, D. P. Principal Domains in Local Correlation Theory. *J. Chem. Theory Comput.* **2019**, *15*, 6597−6606.
(36) Balasubramani, S. G.; Chen, G. P.; Coriani, S.; Diedenhofen, M.; Frank, M. S.; Franzke, Y. J.; Furche, F.; Grotjahn, R.; Harding, M. E.; Hättig, C.; Hellweg, A.; Helmich-Paris, B.; Holzer, C.; Huniar, U.; Kaupp, M.; Marefat Khah, A.; Karbalaei Khani, S.; Müller, T.; Mack, F.; Nguyen, B. D.; Parker, S. M.; Perlt, E.; Rappoport, D.; Reiter, K.; Roy, S.; Rückert, M.; Schmitz, G.; Sierka, M.; Tapavicza, E.; Tew, D. P.; van Wüllen, C.; Voora, V. K.; Weigend, F.; Wodyński, A.; Yu, J. M. TURBOMOLE: Modular program suite for ab initio quantum-chemical and condensed-matter simulations. *J. Chem. Phys.* **2020**, *152*, 184107.
(37) Schmitz, G.; Hättig, C.; Tew, D. P. Explicitly correlated PNO-MP2 and PNO-CCSD and their application to the S66 set and large molecular systems. *Phys. Chem. Chem. Phys.* **2014**, *16*, 22167−22178.
(38) Schmitz, G.; Hättig, C. Perturbative triples correction for local pair natural orbital based explicitly correlated CCSD(F12*) using Laplace transformation techniques. *J. Chem. Phys.* **2016**, *145*, 234107.
(39) Irmler, A.; Burow, A. M.; Pauly, F. Robust Periodic Fock Exchange with Atom-Centered Gaussian Basis Sets. *J. Chem. Theory Comput.* **2018**, *14*, 4567−4580.
(40) Łazarski, R.; Burow, A. M.; Sierka, M. Density Functional Theory for Molecular and Periodic Systems Using Density Fitting and Continuous Fast Multipole Methods. *J. Chem. Theory Comput.* **2015**, *11*, 3029−3041.
(41) Łazarski, R.; Burow, A. M.; Grajciar, L.; Sierka, M. Density functional theory for molecular and periodic systems using density fitting and continuous fast multipole method: Analytical gradients. *J. Comput. Chem.* **2016**, *37*, 2518−2526.
(42) Burow, A. M.; Sierka, M. Linear Scaling Hierarchical Integration Scheme for the Exchange-Correlation Term in Molecular and Periodic Systems. *J. Chem. Theory Comput.* **2011**, *7*, 3097−3104.
(43) Burow, A. M.; Sierka, M.; Mohamed, F. Resolution of identity approximation for the Coulomb term in molecular and periodic systems. *J. Chem. Phys.* **2009**, *131*, 214101.

https://doi.org/10.1021/acs.jctc.5c02179
J. Chem. Theory Comput. 2026, 22, 3927−3936

(44) Müller, C.; Sharma, M.; Sierka, M. Real-time time-dependent density functional theory using density fitting and the continuous fast multipole method. *J. Comput. Chem.* **2020**, *41*, 2573−2582.
(45) Monkhorst, H. J.; Pack, J. D. Special points for Brillouin-zone integrations. *Phys. Rev. B:* **1976**, *13*, 5188−5192.
(46) Zhu, A.; Tew, D. P. Wannier Function Localization Using Bloch Intrinsic Atomic Orbitals. *J. Phys. Chem. A* **2024**, *128*, 8570−8579.
(47) Dunning, T. Gaussian basis sets for use in correlated molecular calculations. I. The atoms boron through neon and hydrogen. *J. Chem. Phys.* **1989**, *90*, 1007−1023.
(48) Woon, D. E.; Dunning, J. r.; Thom, H. Gaussian basis sets for use in correlated molecular calculations. III. The atoms aluminum through argon. *J. Chem. Phys.* **1993**, *98*, 1358−1371.
(49) Peintinger, M. F.; Oliveira, D. V.; Bredow, T. Consistent Gaussian basis sets of triple-zeta valence with polarization quality for solid-state calculations. *J. Comput. Chem.* **2013**, *34*, 451−459.
(50) Vilela Oliveira, D.; Laun, J.; Peintinger, M. F.; Bredow, T. BSSE-correction scheme for consistent gaussian basis sets of double- and triple-zeta valence with polarization quality for solid-state calculations. *J. Comput. Chem.* **2019**, *40*, 2364−2376.
(51) Laun, J.; Bredow, T. BSSE-corrected consistent Gaussian basis sets of triple-zeta valence with polarization quality of the fifth period for solid-state calculations. *J. Comput. Chem.* **2022**, *43*, 839−846.
(52) Weigend, F. Accurate Coulomb-fitting basis sets for H to Rn. *Phys. Chem. Chem. Phys.* **2006**, *8*, 1057−1065.
(53) Sorathia, K.; Tew, D. P. Basis set extrapolation in pair natural orbital theories. *J. Chem. Phys.* **2020**, *153*, 174112.
(54) Sorathia, K.; Frantzov, D.; Tew, D. P. Improved CPS and CBS Extrapolation of PNO-CCSD(T) Energies: The MOBH35 and ISOL24 Data Sets. *J. Chem. Theory Comput.* **2024**, *20*, 2740−2750.
(55) Helgaker, T.; Ruden, T. A.; Jørgensen, P.; Olsen, J.; Klopper, W. A *priori* calculation of molecular properties to chemical accuracy. *J. Phys. Org. Chem.* **2004**, *17*, 913−933.
(56) Werner, K. The principle-quantum-number (and the radial-quantum-number) expansion of the correlation energy of two-electron atoms. *Phys. Chem. Chem. Phys.* **2008**, *10*, 3460−3468.
(57) Perdew, J. P.; Burke, K.; Ernzerhof, M. Generalized Gradient Approximation Made Simple. *Phys. Rev. Lett.* **1996**, *77*, 3865−3868.
(58) Audibert, P.; Sidoumou, M.; Suzanne, J. CO adsorbed on MgO(100): a high resolution LEED study. *Surf. Sci.* **1992**, *273*, L467−L471.
(59) Panella, V.; Suzanne, J.; Hoang, P. N. M.; Girardet, C. CO_2 and CO monolayers on MgO(100): LEED experiments and potential energy calculations. *J. Phys. I France* **1994**, *4*, 905−920.
(60) Shi, B. X.; Rosen, A. S.; Schäfer, T.; Grüneis, A.; Kapil, V.; Zen, A.; Michaelides, A. An accurate and efficient framework for modelling the surface chemistry of ionic materials. *Nat. Chem.* **2025**, *17*, 1688−1695.
(61) Minot, C.; Van Hove, M. A.; Biberian, J.-P. Theory of CO adsorption on MgO(100): the influence of intermolecular interactions on the CO orientation. *Surf. Sci.* **1996**, *346*, 283−293.
(62) Molina, L. M.; Hammer, B. Theoretical study of CO oxidation on Au nanoparticles supported by MgO(100). *Phys. Rev. B* **2004**, *69*, 155424.
(63) Bechthold, P.; Pronsato, M. E.; Pistonesi, C. DFT study of CO adsorption on Pd-SnO2(1 1 0) surfaces. *Appl. Surf. Sci.* **2015**, *347*, 291−298.
(64) Klahn, B.; Bingel, W. A. Completeness and linear independence of basis sets used in quantum chemistry. *Int. J. Quantum Chem.* **1977**, *11*, 943−957.
(65) Ye, H.-Z.; Berkelbach, T. C. Correlation-Consistent Gaussian Basis Sets for Solids Made Simple. *J. Chem. Theory Comput.* **2022**, *18*, 1595−1606.
(66) Guo, Ya-nan; Lu, X.; Zhang, H.-ping; Weng, J.; Watari, F.; Leng, Y. DFT Study of the Adsorption of Aspartic Acid on Pure, N-Doped, and Ca-Doped Rutile (110) Surfaces. *J. Phys. Chem. C* **2011**, *115*, 18572−18581.
(67) Nolan, M. Molecular Adsorption on the Doped (110) Ceria Surface. *J. Phys. Chem. C* **2009**, *113*, 2425−2432.
(68) Lousada, C. M.; Korzhavyi, P. A. Oxygen adsorption onto pure and doped Al surfaces—the role of surface dopants. *Phys. Chem. Chem. Phys.* **2015**, *17*, 1667−1679.
(69) Camarillo-Cisneros, J.; Liu, W.; Tkatchenko, A. Steps or Terraces? Dynamics of Aromatic Hydrocarbons Adsorbed at Vicinal Metal Surfaces. *Phys. Rev. Lett.* **2015**, *115*, 086101.
(70) Starr, D. E.; Campbell, C. T. Large Entropy Difference between Terrace and Step Sites on Surfaces. *J. Am. Chem. Soc.* **2008**, *130*, 7321−7327.
(71) Árnadóttir, Li.; Stuve, E. M.; Jónsson, H. Adsorption of water monomer and clusters on platinum(111) terrace and related steps and kinks. *Surf. Sci.* **2010**, *604*, 1978−1986.
(72) Wandelt, K. Properties and influence of surface defects. *Surf. Sci.* **1991**, *251*−*252*, 387−395.
(73) Ovcharenko, R.; Voloshina, E.; Sauer, J. Water adsorption and O-defect formation on Fe_2 O_3 (0001) surfaces. *Phys. Chem. Chem. Phys.* **2016**, *18*, 25560−25568.
(74) Nasluzov, V. A.; Rivanenkov, V. V.; Gordienko, A. B.; Neyman, K. M.; Birkenheuer, U.; Rösch, N. Cluster embedding in an elastic polarizable environment: Density functional study of Pd atoms adsorbed at oxygen vacancies of MgO(001). *J. Chem. Phys.* **2001**, *115*, 8157−8171.
(75) Fampiou, I.; Ramasubramaniam, A. Binding of Pt Nanoclusters to Point Defects in Graphene: Adsorption, Morphology, and Electronic Structure. *J. Phys. Chem. C* **2012**, *116*, 6543−6555.
(76) Lim, D.-H.; Wilcox, J. DFT-Based Study on Oxygen Adsorption on Defective Graphene-Supported Pt Nanoparticles. *J. Phys. Chem. C* **2011**, *115*, 22742−22747.
(77) Mehmood, F.; Kara, A.; Rahman, T. S.; Henry, C. R. Comparative study of CO adsorption on flat, stepped, and kinked Au surfaces using density functional theory. *Phys. Rev. B* **2009**, *79*, 075422.
(78) Petersen, M. A.; Van Den Berg, J.-A.; Ciobîcă, I. M.; Van Helden, P. Revisiting CO Activation on Co Catalysts: Impact of Step and Kink Sites from DFT. *ACS Catal.* **2017**, *7*, 1984−1992.
(79) Liu, Z.-P.; Hu, P. General Rules for Predicting Where a Catalytic Reaction Should Occur on Metal Surfaces: A Density Functional Theory Study of CH and CO Bond Breaking/Making on Flat, Stepped, and Kinked Metal Surfaces. *J. Am. Chem. Soc.* **2003**, *125*, 1958−1967.
(80) Branda, M. M.; Di Valentin, C.; Pacchioni, G. NO and NO_2 Adsorption on Terrace, Step, and Corner Sites of the BaO Surface from DFT Calculations. *J. Phys. Chem. B* **2004**, *108*, 4752−4758.
(81) Kolb, M. J.; Calle-Vallejo, F.; Juurlink, L. B. F.; Koper, M. T. M. Density functional theory study of adsorption of H2O, H, O, and OH on stepped platinum surfaces. *J. Chem. Phys.* **2014**, *140*, 134708.
(82) Wan, K.; He, J.; Shi, X. Construction of high accuracy machine learning interatomic potential for surface/interface of nanomaterials—a review. *Adv. Mater.* **2024**, *36*, 2305758.
(83) Focassio, B.; M Freitas, L. P.; Schleder, G. R. Performance assessment of universal machine learning interatomic potentials: Challenges and directions for materials' surfaces. *ACS Appl. Mater. Interfaces* **2025**, *17*, 13111−13121.

https://doi.org/10.1021/acs.jctc.5c02179
J. Chem. Theory Comput. 2026, 22, 3927−3936